PLOS ONE

RESEARCH ARTICLE

Computational analysis of the metal selectivity of matrix metalloproteinase 8

Zheng Long *

Department of Chemistry and Biochemistry, University of California San Diego, San Diego, California, United States of America

* longzheng26@gmail.com

Abstract

Matrix metalloproteinase (MMP) is a class of metalloenzyme that cleaves peptide bonds in extracellular matrices. Their functions are important in both health and disease of animals. Here using quantum mechanics simulations of the MMP8 protein, the coordination chemistry of different metal cofactors is examined. Structural comparisons reveal that Jhan-Teller effects induced by Cu(II) coordination distorts the wild-type MMP8 active site corresponding to a significant reduction in activity observed in previous experiments. In addition, further analysis suggests that a histidine to glutamine mutation at residue number 197 can potentially allow the MMP8 protein to utilize Cu(II) in reactions. Simulations also demonstrates the requirement of a conformational change in the ligand before enzymatic cleavage. The insights provided here will assist future protein engineering efforts utilizing the MMP8 protein.

Citation: Long Z (2020) Computational analysis of the metal selectivity of matrix metalloproteinase 8. PLoS ONE 15(12): e0243321. https://doi.org/10.1371/journal.pone.0243321

Editor: Eugene A. Permyakov, Russian Academy of Medical Sciences, RUSSIAN FEDERATION

Received: July 20, 2020

Accepted: November 18, 2020

Published: December 4, 2020

Data Availability Statement: All the related data files have been submitted to: https://doi.org/10.7910/DVN/KNHVVX.

Funding: The author received no specific funding for this work.

Competing interests: The author have declared that no competing interests exist.

Introduction

Matrix metalloproteinase (MMP) is a class of proteins whose native functions involves the processing of extracellular matrix and cytokines [1,2]. As a result they are essential for the signal transduction pathway in immune cells signaling. MMPs have been used in anti-cancer clinical trials[3], however, their functions and involvements in cancer has not been fully understood. Despite recent setbacks in clinical efforts, MMPs are still considered viable targets in cancer therapies, but the focus has been given to the targeting specificity of highly analogous MMPs [4]. One of the poorly understood areas for the MMP proteins is the structure-function relationship between their active site metal selectivity and ligand selectivity. Better understanding of MMP protein metal selectivity can thus help to elucidate the behaviors of these proteins in healthy tissues as well as disease environments. The aim of this work is to use computational methods to provide insights into the metal selectivity of the MMPs to assist future efforts to engineer MMPs that may serve therapeutic functions.

All MMPs contain three important domains, the pro-domain, catalytic domain and hemopexin like domain. The catalytic domain of MMPs are sufficient for their enzymatic cleavage [1]. It is known that Zn(II) bound to MMPs catalytic domain can be substituted by Cu(II), Co (II), Mg(II), and Mn(II). In addition, activities of MMPs varies with different metals as well as

their concentration [5]. These previously published results are tabulated in Table 1. The variation in MMP catalytic activities not only show that the cofactor dependent chemistry is not unique to Zn(II) ions, but that the activities are highly biased in MMPs favoring certain metal ions. In experimental data, Mg(II) has slightly lower activities compared to Zn(II), in contrast, Cu(II) demonstrates almost no activity at the concentration of 10 mM. Because 10 mM is still higher than physiologically relevant metal concentration in the body [6,7], it is reasonable to expect more dramatic differences *in vivo*.

In MMPs, selectivity of divalent metals is not evident from the coordination site structures, for similar coordination chemistry can be found in proteins harboring different divalent metal ions [8,9]. Experimental data suggests that there is physiological relevance of MMP proteins utilizing Cu(II) as a cofactor, this is despite Cu(II) MMP seem to demonstrate no collagenase activities under normal conditions. In fact, it was shown that MMPs can process new ligands in the presence of Cu(II) [10–12], this suggests that changing metal cofactors in MMPs alters ligand selectivity as well. Interestingly, there exist a variant metalloproteinase favoring Cu(II) instead of Zn(II), which can serve as a comparison to the MMPs.

The discovery and characterization of a new family of metalloproteinase in the green algea *Volvox carteri* named the VMP3 reveal a similar metal coordination motif of QEXXHXXGXXH instead of the HEXXHXXGXXH in the MMPs, and the discovery that this motif favors the utilization of copper in catalysis [13] suggests that a similar mutation in the MMPs can alter Zn(II) and Cu(II) selectivity in the MMP catalytic site metal binding pocket. Comparing the coordination chemistry of the two proteins might reveal the mechanism behind metal selectivity of MMPs and VMP3. However, there are currently no experimental structures available for VMP3. Since VMP3 shares only about 20% homologies to MMPs, direct modeling of the VMP3 based on existing MMP structures is not possible. Instead, a homology model was generated for the apo VMP3 using IntFold based on homologies of VMP3 domains with other analogous proteins and strcutrual domains available in the protein crystal structure database[14]. The structure of the predicted VMP3 protein is shown in Fig 1A. The QEXXHXXGXXH motif is shown arranged spatially similar to that of MMP8 (Fig 1B). Compared to VMP proteins, MMP proteins has been studied extensively, and many structures exist for MMPs.

In humans, there are at least 10 MMP proteins: MMP1, MMP2, MMP3, MMP7, MMP8, MMP9, MMP10, MMP11, MMP20, and MMP26. MMP8 or neutrophil metalloproteinase is expressed on neutrophils to remodel the extracellular matrix allowing immune cell infiltrate tissues. It is believed to possess anti-cancer effects by allowing immune cell penetration into the cancer microenvironments. MMP8 itself is involved in tumor survival and mobility, its expression is associated with both pro and anti-tumor effects in different types of tumor environments [15]. Understandings of the functional metal coordination of the MMP catalytic sites can help to elucidate the effects of divalent metals as well as mutations over the ligand selectivity of the MMP proteins in different disease environments. Because of the importance of MMP8 in disease, it is used as a representative MMP protein for simulations. In addition,

Table 1. Results for metal activities against collagen [5].

Metal Ion Species	Activity (100 mM Ion)	Activity (10 mM Ion)
Zn(II)	98.5%	32.3%
Cu(II)	41.5%	0%
Mg(II)	100%	23%
Co(II)	89.2%	15.4%
Mn(II)	90.8%	7.7%

https://doi.org/10.1371/journal.pone.0243321.t001

due to the disease relevance of Cu(II) in cancer where it is found that the concentration of Cu (II) is elevated in tumor tissues [7, 16,17], focus has also been given to the effects of Cu(II) cofactor on the structures of the MMP8 protein.

The MMP8 protein contains two Zn(II) binding sites. Site I has four residues of H147, D149, H162, and H175 forming a tetrahedral coordination site with the zinc ion. Site II has three residues H197, H201, and H207 forming a zinc binding site with the motif HEXXHXXGXXH. Site II is the catalytic site in MMP8 where peptide bond cleavage takes place. The motif in site II is not just found in other MMPs but also common to a family of enzymes named metzinsins [18]. Because of the conserved catalytic site structures across different MMPs, the chemistry of MMPs can be readily modeled base on the coordination sites around the metal center, and the results can be readily applied to other proteins within the class.

Close examination of the crystal structure of inhibitor bound MMP8 reveals that the zinc ion in the catalytic site is coordinated by three histidine residues and one catechol inhibitor N-(3,4-dihydroxyphenyl)-4-diphenylsulfonamide [19]. This crystal structure of MMP8 is shown in Fig 1A. In the coordination center highlighted in the boxed area, Zn(II) is stabilized by the addition of coordinating inhibitors. In the absence of the inhibitors or ligands, the coordination site is believed to be satisfied by a water molecule which can be polarized by the adjacent glutamate residue next to one of the coordinating histidine residues. This has been demonstrated in the inhibitor-free MMP-12 structure [20] and in MMP-3 [21–23] previously. These knowledge forms the basis of the modeling performed in this work on MMP8, because the structures of the catalytic sites of all MMPs are conserved, metal coordination chemistry is believed to be conserved for all MMPs [1].

MMP ligand interactions has been studied using x-ray crystallography and nuclear magnetic resonance spectroscopy [24,25]. Using these structural information, the direction of the ligand-MMP interactions can be identified. In addition, previous simulations have suggested that the ligand coordination likely occurs in a bi-dentate fashion [21]. These prior knowledge enables the correct modeling of the ligand structure at the MMP8 catalytic site.

There is no crystal structure for copper bound MMP proteins but similar copper proteins exist. Plastocyanins contain a type I copper center [26] which is formed by two histidine residues, one cysteine, and one methionine into a distorted tetrahedral coordination center

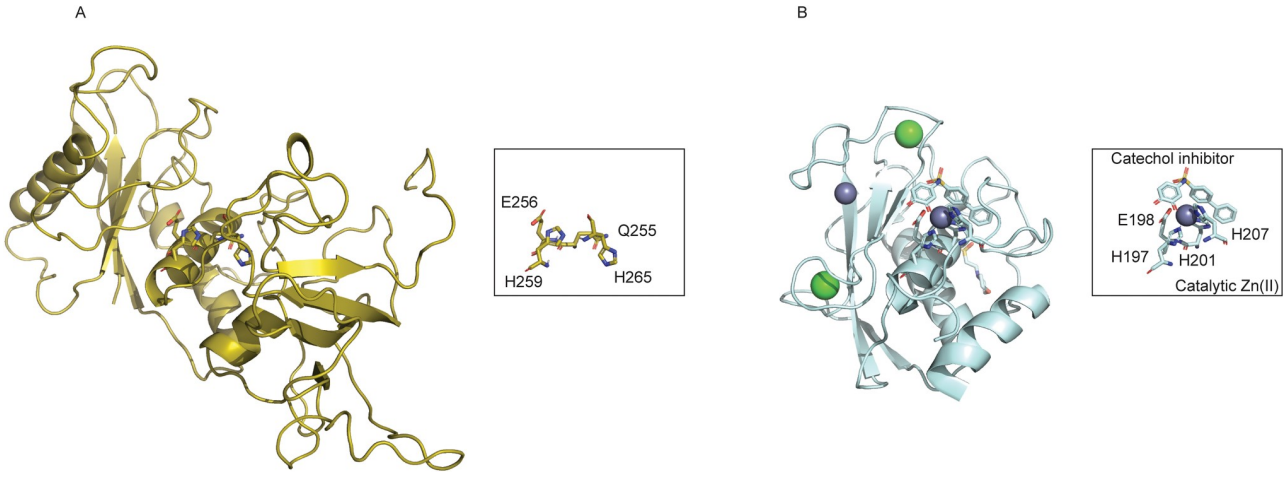

Fig 1. (A) Homology modeled apo VMP3 structure predicted using IntFold [14]. (B) Inhibited form of the MMP8 catalytic domain crystal structure (5h8x) [19], the rectangular box highlights the catalytic site in MMP8 with the Zn(II) ion. The rectangular box highlights the catalytic site in VMP3 without any metal ion.

https://doi.org/10.1371/journal.pone.0243321.g001

around the Cu(II) ion. The three histidine coordination for Cu(II) typically has pyramidal coordination involving a second Cu(II) nearby bonding to each other through the tips (type III copper center) [26]. For proteins like plastocyanin, metal requirements are also non-exclusive [27]. In azurins for example, Zn(II) occupied active site instead of the native Cu(II) remains functional, however, a geometry distortion was observed in the Zn(II) occupied protein [28]. These results suggest that in proteins utilizing divalent metals as cofactors, the metal species are often times non-exclusive but the presence of non-native metal ions is still disruptive to the coordination geometry.

Using computational simulations, it is possible to understand the behaviors of MMPs and make predictions of effects due to changes in the coordination centers. These approaches have been instrumental for studies of metal coordination chemistry within proteins. Metal coordination chemistry requires the use of quantum mechanics (QM) simulations, for the traditional force fields have not been able to completely address the chemistry around these metal co-factors [29]. Previous study has identified the presence/absence of metal binding selectivity in various type of divalent metal metalloproteins using molecular dynamics simulations, this approach, however, does not provide enough accuracy in comparisons of structural differences induced by different divalent metal cofactors [30]. Density functional theory (DFT) has been applied to the studies of protein, which provides sufficient computational efficiency as well as accuracy. But compared to molecular dynamics simulations, only part of the protein can be simulated efficiently and thus this general approach is applied here to only simulate around the first coordination shell around the metal coordination center [31]. The QM approach undertaken here is beneficial for the close examination of the local coordination chemistry, however, it largely misses the other protein-protein interactions important for ligand selectivity as well as complex stability, thus the scope of this work is limited to the events around the coordination center, and a more sophisticated approach using the QM/MM methods has to be utilized to understand the behavior of the MMPs systematically [32].

Materials and methods

Catalytic site modeling is performed in PyMol. Computations were performed with a Linux system equipped with a NVidia Tesla K10 GPU. DFT Geometry optimization were performed with B3LYP/LANL2DZ level of theory as previously [21] in Gaussian 09 [33] to obtain better computational efficiency. Canonical molecular orbitals calculated with the same levels of theory were visualized in GaussView 5.0 [34] using B3PW91/6-311G++3df,3dp methods. All the related data files have been submitted to: https://doi.org/10.7910/DVN/KNHVVX.

Structural modeling was carried out starting from the Zn(II) catalytic site for MMP8 in crystal structure [19] and the position of the water molecule was modeled in before geometry optimization based on the previous structures and structural models [20, 25]. At the edge of the computational boundary, the Cα atoms of the amino acid residues are replaced by methyl groups, and the carbon atom is frozen in calculation to prevent forbidden backbone angles without the contextual restraints. This approach is chosen based on the observation that there are no separate conformations for *apo* and ligand bound/inhibited form of the MMP protein [19, 25]. Ligand modeling was based on the crystal structure of the collagen III derived peptides [35] which contain known cleavage sites for MMP8 and structural models of MMP collagen interactions [25].

Results and discussion

To understand the differential activities of divalent metal ions, computational methods were used to elucidate the molecular mechanism of the metal biases. First, coordination geometries

of different metals in the catalytic site was examined after performing a series of geometry optimizations. Initial guesses of these calculations were all modeled based on the MMP8 crystal structure containing the Zn(II) cofactor (Fig 2). Two major types of coordination geometries resulted from the simulations can be identified in the catalytic site in the absence of E198 or ligands. Co(II), Cu(II) and Ni(II) coordination geometries are similar to square planner while Ca(II), Zn(II), Mg(II) and Mo(II) geometries are similar to tetrahedral. Mn(II) coordination geometry, however, resides between the two cases.

In the calculations, the catalytic site was simplified such that calculations are efficient but still representative of the coordination chemistry around the metal center. In the modeling, the alpha carbons were converted to methyl groups to prevent unrealistic destabilization at the simulation boundaries. In addition, restraints were added to the system to prevent the residues from deviating from their natural orientations. The observation that different metal ions all have distinctive geometries in the simulations is expected and suggests ligand selectivity is dictated to some levels by the coordination chemistry of the metals and such differences might be correlated with the functional differences demonstrated by these metals. Geometric differences around the coordination sites are observed while the C_α atoms of the amino acid residues are fixed, indicating that these rearrangements can be accommodated by local side-chain conformational rearrangements and thus does not necessarily require backbone movements. These fixed atoms are also important for they can prevent unrealistic geometries which may require sterically forbidden backbone conformations, and it is especially important for subsequent calculations where additional residues are included which can further complicate the energy landscape.

In the ligand-free protein, the effects of the H197Q mutation is examined to determine if the mutation is structurally viable. Simulations show that this mutation can fit within the catalytic site of MMP8 without requiring protein backbone changes (Fig 3). Simulations of the H197Q mutants also show that coordination geometries around Cu(II) and Zn(II) are changed due to changed coordinating chemical groups. In Fig 3 it can be seen that, compare to the wild-type protein (Fig 2A–2D), H197Q mutant has distortion of the coordination geometry of the Zn(II) or Cu(II) cofactors due to the way Q197 approaches the metal center. These differences are consistent with observations when ligand is included in the simulations.

Inclusion of E198 in the calculations distorts both the wild-type and mutant coordination geometries (Fig 4). In the wild-type protein, E198 side-chain draws the water molecule closer to itself, thus changing the coordination angles (Fig 4A–4D). Similar effects are seen in H197Q mutant with Cu(II) center (Fig 4G and 4H). The distortions caused by E198 reduces the coordination geometries differences between wild-type or H197Q mutant catalytic site. However, after including E198 in simulations, the coordination geometries of Zn(II) occupied MMP8 H197Q catalytic site produces an additional hydrogen bond formed between E198 carbonyl oxygen atom and Q197 side-chain ε amino group (Fig 4E and 4F). This hydrogen bond changes the relative positions of residue H207 to residue 197. In contrast, hydrogen bonding interactions are absent when Cu(II) is present in the mutant catalytic site (Fig 4G and 4H). Such inter-residue hydrogen bonding interactions are also absent in wild-type MMP8 catalytic site with Cu(II) or Zn(II) occupancy.

In addition to the inclusion of E198, ligand binding further alters the coordination geometry (Fig 5A–5D). The coordination of the ligand in the native Zn(II) occupied MMP8 catalytic site forms a distorted octahedral geometry which involves bidentate coordination from two adjacent ligand carbonyl groups. From the two types of coordination geometries observed in the ligand-free simulations (Fig 2), additional metal ions Mg(II) and Co(II) (Fig 5E–5H) were selected as comparisons to Zn(II) and Cu(II) (Fig 5A–5D). Results show that similar to the ligand-free simulations, the coordination geometry of Mg(II)-MMP-ligand complex is similar to that of the Zn(II)-MMP8-ligand geometry while Co(II)-MMP8-ligand geometry resembling

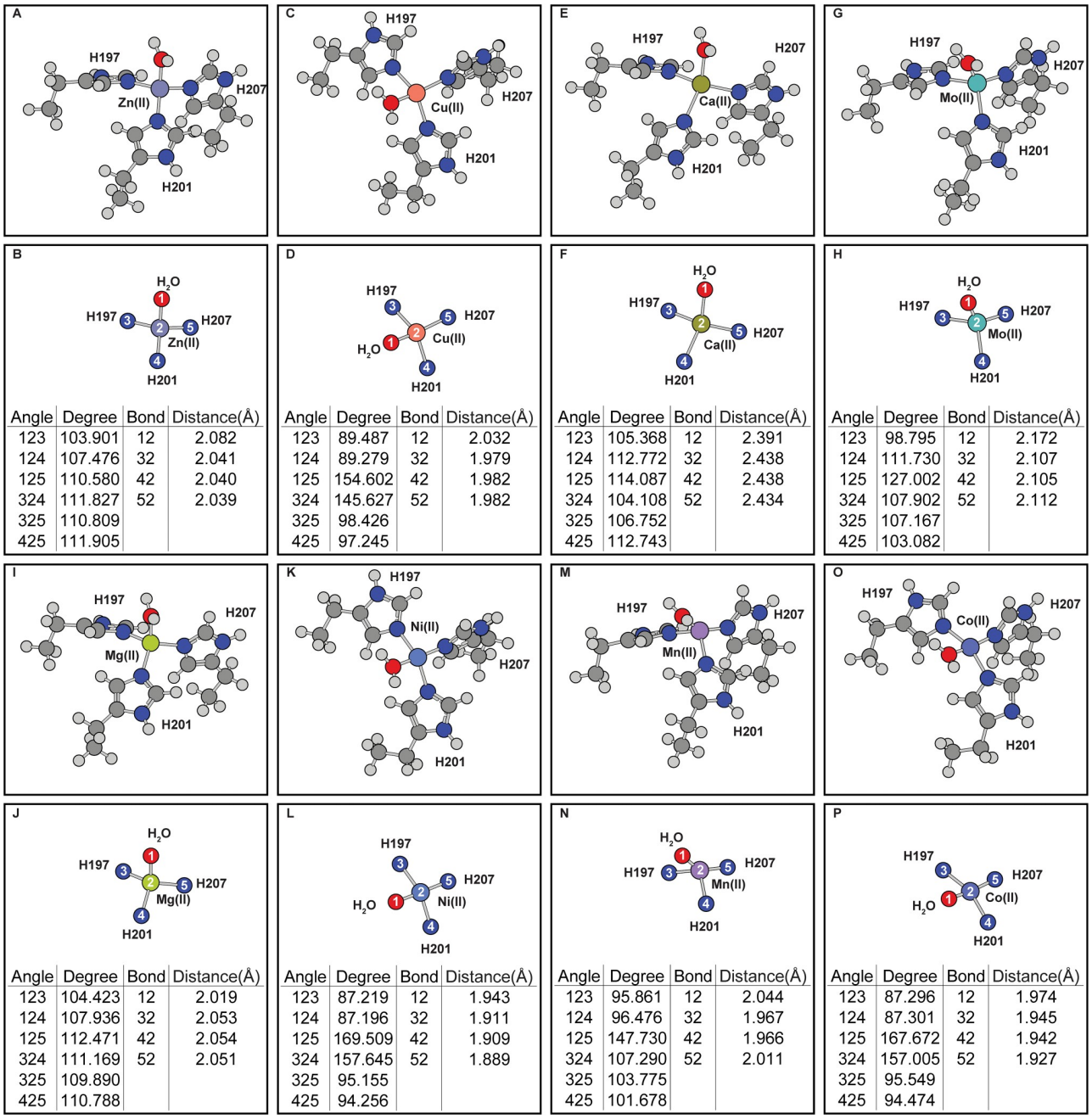

Angle	Degree	Bond	Distance(Å)
123	103.901	12	2.082
124	107.476	32	2.041
125	110.580	42	2.040
324	111.827	52	2.039
325	110.809		
425	111.905		

Angle	Degree	Bond	Distance(Å)
123	89.487	12	2.032
124	89.279	32	1.979
125	154.602	42	1.982
324	145.627	52	1.982
325	98.426		
425	97.245		

Angle	Degree	Bond	Distance(Å)
123	105.368	12	2.391
124	112.772	32	2.438
125	114.087	42	2.438
324	104.108	52	2.434
325	106.752		
425	112.743		

Angle	Degree	Bond	Distance(Å)
123	98.795	12	2.172
124	111.730	32	2.107
125	127.002	42	2.105
324	107.902	52	2.112
325	107.167		
425	103.082		

Angle	Degree	Bond	Distance(Å)
123	104.423	12	2.019
124	107.936	32	2.053
125	112.471	42	2.054
324	111.169	52	2.051
325	109.890		
425	110.788		

Angle	Degree	Bond	Distance(Å)
123	87.219	12	1.943
124	87.196	32	1.911
125	169.509	42	1.909
324	157.645	52	1.889
325	95.155		
425	94.256		

Angle	Degree	Bond	Distance(Å)
123	95.861	12	2.044
124	96.476	32	1.967
125	147.730	42	1.966
324	107.290	52	2.011
325	103.775		
425	101.678		

Angle	Degree	Bond	Distance(Å)
123	87.296	12	1.974
124	87.301	32	1.945
125	167.672	42	1.942
324	157.005	52	1.927
325	95.549		
425	94.474		

Fig 2. Effects of divalent metal occupancy on the MMP8 catalytic center without E198 or ligand. (A-B) Zn(II). (C-D) Cu(II). (E-F) Ca(II). (G-H) Mo(II). (I-J) Mg(II). (K-L) Ni(II). (M-N) Mn(II). (O-P) Co(II). (A), (C), (E), (G), (I), (K), (M), and (O) are the full coordination shell. (B), (D), (F), (H), (J), (L), (N) and (P) contain simplified depictions showing only atoms directly coordinated with the metals, as well as tables for the angles and distances of the coordination center.

https://doi.org/10.1371/journal.pone.0243321.g002

that of the Cu(II)-MMP8-ligand geometry. From the geometry of the Cu(II)-MMP8-ligand structure, the coordination of the ligand is somewhat incompatible with the coordination site, because the i-1 ligand does not seem to be able to get close to the metal. In the Cu(II) occupied wild-type MMP8 catalytic site, the coordination bond between Cu(II) and carbonyl oxygen atom of the ligand at i position extends to 3.35 Å which is significantly larger than the regular

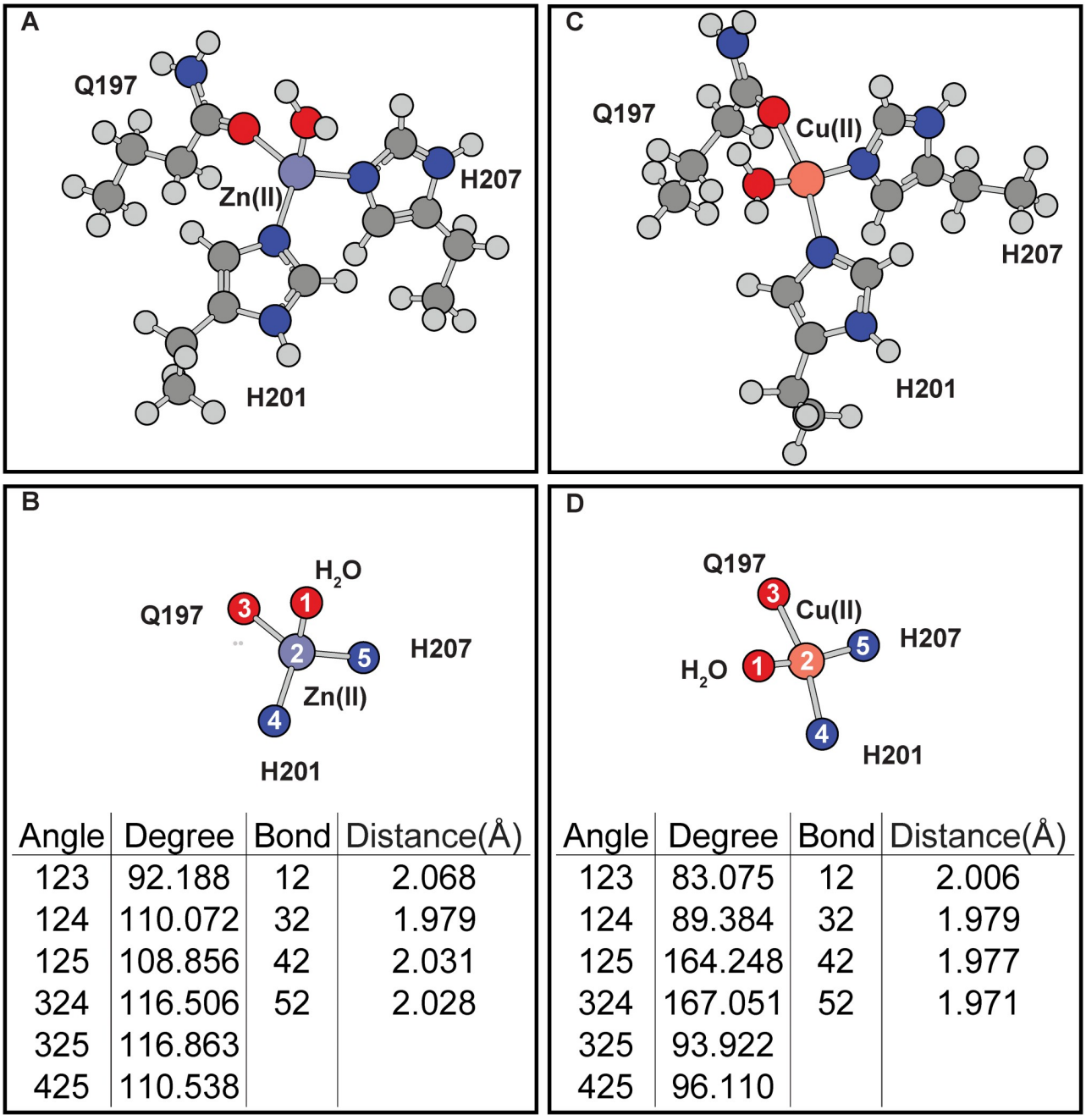

Angle	Degree	Bond	Distance(Å)
123	92.188	12	2.068
124	110.072	32	1.979
125	108.856	42	2.031
324	116.506	52	2.028
325	116.863		
425	110.538		

Angle	Degree	Bond	Distance(Å)
123	83.075	12	2.006
124	89.384	32	1.979
125	164.248	42	1.977
324	167.051	52	1.971
325	93.922		
425	96.110		

Fig 3. Effects of H197Q mutation on the coordination geometry of the MMP8 catalytic site without E198 or ligand. (A-B) Zn(II). (C-D) Cu(II). (A) and (C) are the full coordination shell. (B) and (D) contain simplified depictions showing only atoms directly coordinated with the metals, as well as tables for the angles and distances of the coordination center.

https://doi.org/10.1371/journal.pone.0243321.g003

coordination bonds in the range of 2.00–2.50 Å distance range measured in structures containing other metal ions.

The differences in coordination geometry due to histidine to glutamine mutation is expected because the two amino acids contain sidechains that are very different in coordination properties. Strong Jahn-Teller effect, indicated by the distortion of Cu(II)–ligand$_i$ bond

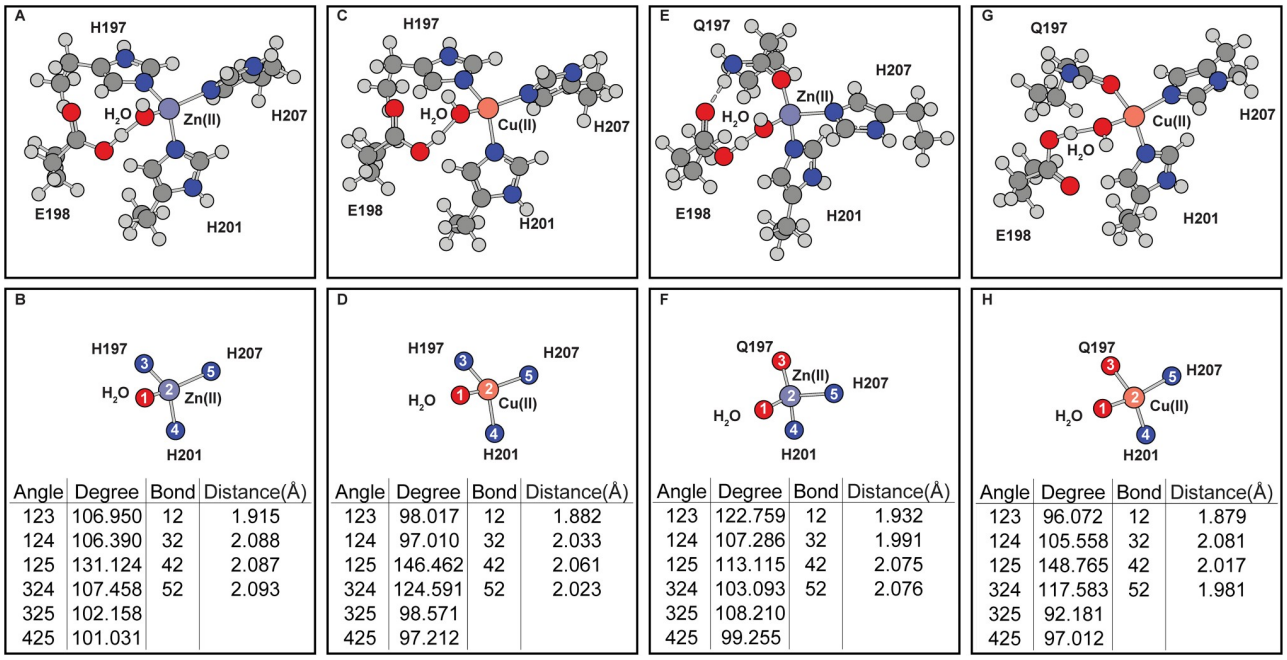

Angle	Degree	Bond	Distance(Å)
123	106.950	12	1.915
124	106.390	32	2.088
125	131.124	42	2.087
324	107.458	52	2.093
325	102.158		
425	101.031		

Angle	Degree	Bond	Distance(Å)
123	98.017	12	1.882
124	97.010	32	2.033
125	146.462	42	2.061
324	124.591	52	2.023
325	98.571		
425	97.212		

Angle	Degree	Bond	Distance(Å)
123	122.759	12	1.932
124	107.286	32	1.991
125	113.115	42	2.075
324	103.093	52	2.076
325	108.210		
425	99.255		

Angle	Degree	Bond	Distance(Å)
123	96.072	12	1.879
124	105.558	32	2.081
125	148.765	42	2.017
324	117.583	52	1.981
325	92.181		
425	97.012		

Fig 4. Effects of E198 on the MMP8 catalytic center without ligand. (A-B) Zn(II) occupied wild-type MMP8. (C-D) Cu(II) occupied wild-type MMP8. (E-F) Zn(II) occupied MMP8 H197Q mutant. (G-H) Cu(II) occupied MMP8 H197Q mutant. (A), (C), (E), and (G) are the full coordination shell. (B), (D), (F), and (H) contain simplified depictions showing only atoms directly coordinated with the metals, as well as tables for the angles and distances of the coordination center.

https://doi.org/10.1371/journal.pone.0243321.g004

and the elongation of the Cu(II)–ligand$_{i-1}$ bond (Fig 5C and 5D) is observed in Cu(II) occupied wild-type MMP8 active site. Similar Jahn-Teller effect is observed in Co(II) occupied wild-type MMP catalytic site although to a lesser extent. Jahn-Teller effect in Cu(II) occupied H197Q MMP8 mutant (Fig 6C and 6D) on the other hand is reflected in the elongation of the Cu(II)–ligand$_i$ and Cu(II)–H201 bonds. Distortion is also observed in Zn(II) occupied H197Q mutant in the presence of the ligand, this is due to the formation of a hydrogen bond between the side-chain NH_2 group with the ligand carbonyl oxygen at position i. These distortions constitute the metal selectivity of the MMP protein catalytic site.

The consequences of the distortions in the Cu(II) occupied protein is significant. Compared to the H197Q mutant, wild-type catalytic site contains ligand coordination bond that stretches to 3.35 Å. This prevents the orbital hybridization between the orbitals of the Cu(II) ion with the orbitals of the carbonyl oxygen atom. This is demonstrated in S1 Fig where the molecular orbitals containing all the bonding orbitals between the Cu(II) and ligand atoms are shown, Cu(II) in wild-type MMP8 catalytic site has no bonding electron density between Cu(II) and the carbonyl oxygen atom at ligand position i-1. As a result, this complex can be expected to be less stable. Thus, it can be suggested here that the Jahn-Teller distortions in Cu(II) bound MMP8 may destabilize the coordination center. The effect of the hydrogen bonding in Zn(II) occupied H197Q mutant also elongates the metal–ligand bond to 2.77 Å which still allows orbital hybridization revealed by similar molecular orbital analysis, although the bonding molecular orbitals reduces from twelve in wild-type MMP8 to seven in the H197Q mutant. As a result, conclusion cannot be drawn about the effect of the mutation on the stability of the Zn (II) bound MMP8 H197Q.

Close examination of the distances between the water oxygen atom and the ligand carbonyl carbon atom at ligand position i where cleavage takes place, shows that this distance is around

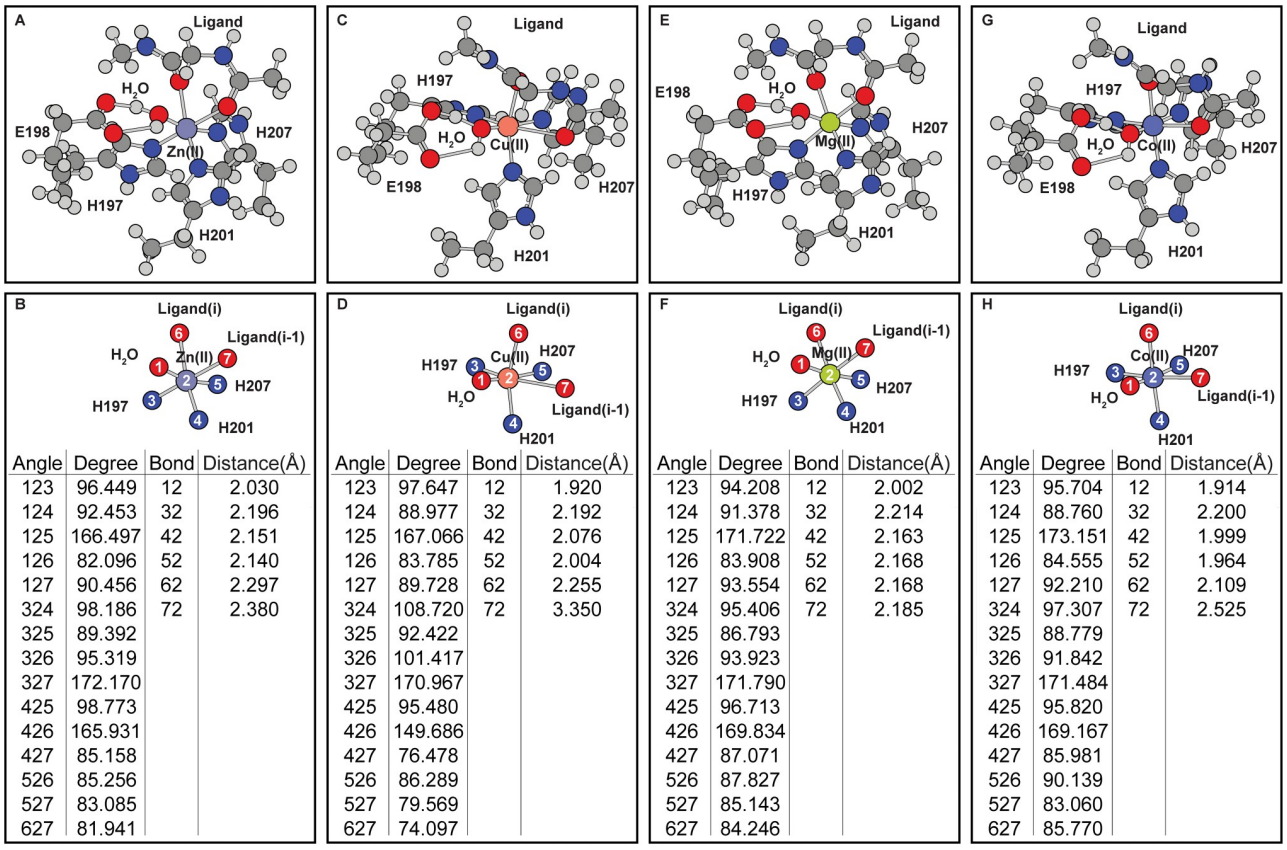

Angle	Degree	Bond	Distance(Å)
123	96.449	12	2.030
124	92.453	32	2.196
125	166.497	42	2.151
126	82.096	52	2.140
127	90.456	62	2.297
324	98.186	72	2.380
325	89.392		
326	95.319		
327	172.170		
425	98.773		
426	165.931		
427	85.158		
526	85.256		
527	83.085		
627	81.941		

Angle	Degree	Bond	Distance(Å)
123	97.647	12	1.920
124	88.977	32	2.192
125	167.066	42	2.076
126	83.785	52	2.004
127	89.728	62	2.255
324	108.720	72	3.350
325	92.422		
326	101.417		
327	170.967		
425	95.480		
426	149.686		
427	76.478		
526	86.289		
527	79.569		
627	74.097		

Angle	Degree	Bond	Distance(Å)
123	94.208	12	2.002
124	91.378	32	2.214
125	171.722	42	2.163
126	83.908	52	2.168
127	93.554	62	2.168
324	95.406	72	2.185
325	86.793		
326	93.923		
327	171.790		
425	96.713		
426	169.834		
427	87.071		
526	87.827		
527	85.143		
627	84.246		

Angle	Degree	Bond	Distance(Å)
123	95.704	12	1.914
124	88.760	32	2.200
125	173.151	42	1.999
126	84.555	52	1.964
127	92.210	62	2.109
324	97.307	72	2.525
325	88.779		
326	91.842		
327	171.484		
425	95.820		
426	169.167		
427	85.981		
526	90.139		
527	83.060		
627	85.770		

Fig 5. Effects of divalent metal occupancy on the ligand bound MMP8 catalytic center. (A-B) Zn(II). (C-D) Cu(II). (E-F) Mg(II). (G-H) Co(II). (A), (C), (E), and (G) are the full coordination shell. (B), (D), (F), and (H) contain simplified depictions showing only atoms directly coordinated with the metals, as well as tables for the angles and distances of the coordination center.

https://doi.org/10.1371/journal.pone.0243321.g005

2.8–2.9 Å in all of the calculated structures (S1 Table). Mutations and metal induced changes does not change this distance significantly. As a result, no implications can be made to the reaction rate based on the simulations. Furthermore, due to the lack of information about the mechanisms of the induced transition state, i.e. whether it is due to dynamic changes in the MMP protein or due to changes in ligand orientation, a confident prediction of the transition state structure was not sought here using simulations.

Compared to the functional data shown in Table 1 which shows that the activities of Mg(II) is slightly lowered than Zn(II) at 10 mM concentration, simulation shows Mg(II) demonstrates very similar coordination geometry in MMP8. In contrast, Cu(II) has no activities against collagen at 10 mM concentration. Simulation shows that Cu(II) significantly alters the ligand-metal-MMP8 complex. In experiments, Co(II) has higher activities than Cu(II) against collagen but much lower activities than Mg(II) or Zn(II), this is compared to the simulations where the Co(II) bound MMP8 experiences less distortion effect compared to Cu(II) bound protein.

Active site mutants of the MMP protein has been made experimentally. The mutation in the active site motif from HEXXHXXGXXH to HQXXHXXGXXH has been studied. This is a loss-of-function mutation that diminishes the catalytic activities of the MMP proteins, and the structure of the mutant is comparable to that of the wild-type protein [36]. In contrast experimental results for QEXXHXXGXXH mutations does not exist, so functional comparisons can only be made with the VMP3 protein which harbors a naturally functional QEXXHXXGXXH

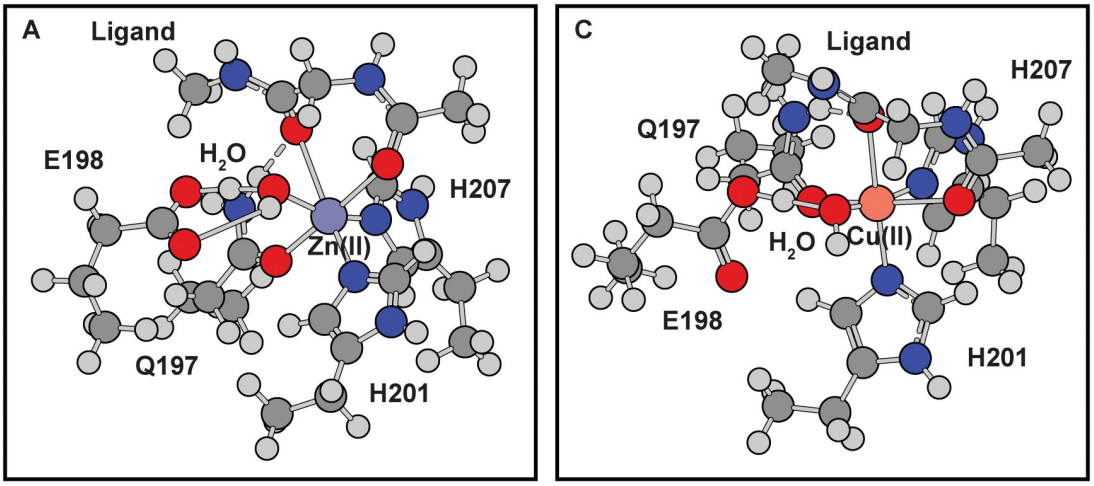

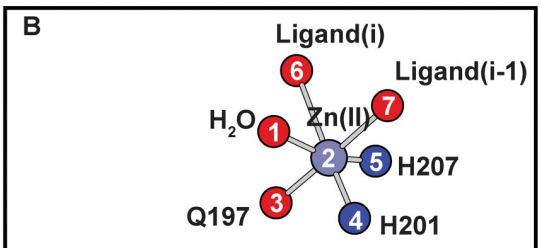

Angle	Degree	Bond	Distance(Å)
123	90.958	12	2.005
124	99.534	32	2.138
125	156.264	42	2.097
126	75.631	52	2.121
127	94.277	62	2.766
324	94.310	72	2.223
325	86.418		
326	91.561		
327	170.558		
425	104.184		
426	172.473		
427	92.568		
526	80.859		
527	85.629		
627	82.158		

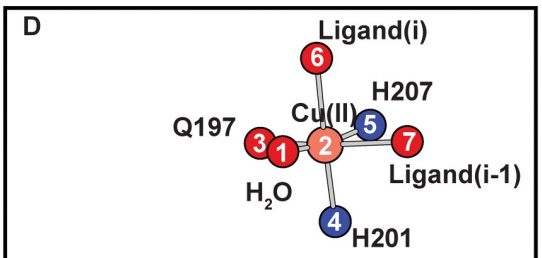

Angle	Degree	Bond	Distance(Å)
123	94.527	12	1.921
124	90.495	32	2.227
125	170.268	42	2.048
126	81.408	52	2.001
127	94.252	62	2.359
324	95.538	72	2.545
325	87.841		
326	93.382		
327	170.971		
425	98.681		
426	168.400		
427	86.488		
526	89.037		
527	83.153		
627	85.849		

Fig 6. Effects of H197Q mutations on the ligand bound MMP8 catalytic center. (A-B) Zn(II). (C-D) Cu(II). (A) and (C) are the full coordination shell. (B) and (D) contain simplified depictions showing only atoms directly coordinated with the metals, as well as tables for the angles and distances of the coordination center.

https://doi.org/10.1371/journal.pone.0243321.g006

motif favoring Cu(II). The observation that in the H197Q mutant, which is analogues to VMP3, Cu(II) induces a more stable coordination structure than in wild-type MMP8 by allowing an additional ligand coordination bond suggest that the H197Q might demonstrate similar metal selectivity to VMP3 where Cu(II) will have much better utilization.

The computations also suggest that favorable ligand torsion angles for metal coordination deviates from that measured in collagen crystal structures. These torsion angle changes are measured and shown in S2 Table showing comparisons of the angles found in geometry optimized structures to the starting structure of collagen III. Previous studies hypothesize that partial refolding of the collagen might occur leading to collagen cleavage [24], this matches previous results showing that the torsion angles of the bound ligand changes significantly. Ligand binding to the active site metal can potentially induce structural changes in MMPs as well. However, based on the simulations, large domain conformational changes might not be required, for side-chain rearrangements can be sufficient to accommodate these local changes.

Evidence suggest Cu(II) does lead to additional substrate proteolysis in MMPs compared to Zn(II) [11] these effects are reflected in the selectivity of torsion angles for different ligands, limited modeling capabilities of the QM simulations likely means that simulating larger segments of the MMP proteins complexed with a more contextual ligand will remain difficult. This can potentially be overcome using novel potential energy functions in MM simulations and QM/MM methods [37].

Conclusions

Computational analysis provides insights into the behaviors of MMP8 protein in the presence of different metal cofactors. In particular, the coordination geometries of the Zn(II) and Cu(II) occupied MMP8 are predicted and examined. It is found that Jhan-Teller effects alter the Cu (II) occupied MMP8 by changing ligand binding from a bi-dentate to a mono-dentate fashion. In addition, simulations predict that H197Q is likely going to be able to utilize Cu(II) in catalytic reactions. In simulations, favorable ligand torsion angles at the enzyme cleavage position are predicted, and the optimized angles were found to differ from those measured in the crystal structure of collagen ligand, suggesting that a ligand conformational change is required before MMP8 cleavage can take place. The insights provided by these simulations provides directions for future protein engineering efforts based on the MMP8 protein.

Supporting information

S1 Fig. Cu(II) –ligand orbital mixing the bonding orbitals formed between the ligand and Cu(II) ion. (A) is a molecular representation of the Cu(II)-ligand complex in wild-type MMP8 catalytic site. (B)-(D) are three bonding molecular orbitals between Cu(II) and ligand wild-type MMP8 catalytic site. (E) is a molecular representation of the Cu(II)-ligand complex in H197Q mutant catalytic site. (B)-(D) are four bonding molecular orbitals between Cu(II) and ligand in H197Q mutant catalytic site.
(TIF)

S1 Table. Relative distance between the water oxygen atom and the carbonyl carbon atom.
(DOCX)

S2 Table. Torsion angles in the simulated ligand for the i position where peptide bond gets cleaved by MMP8.
(DOCX)

Author Contributions

Writing – original draft: Zheng Long.

References

1. Nagase H, Woessner JF Jr. Matrix metalloproteinases. J Biol Chem. 1999; 274(31):21491–4. https://doi.org/10.1074/jbc.274.31.21491 PMID: 10419448
2. Kleiner DE Jr., Stetler-Stevenson WG. Structural biochemistry and activation of matrix metalloproteases. Curr Opin Cell Biol. 1993; 5(5):891–7. https://doi.org/10.1016/0955-0674(93)90040-w PMID: 8240832
3. Overall CM, Lopez-Otin C. Strategies for MMP inhibition in cancer: innovations for the post-trial era. Nat Rev Cancer. 2002; 2(9):657–72. https://doi.org/10.1038/nrc884 PMID: 12209155
4. Fields GB. The Rebirth of Matrix Metalloproteinase Inhibitors: Moving Beyond the Dogma. Cells. 2019; 8(9). https://doi.org/10.3390/cells8090984 PMID: 31461880
5. Macartney HW, Tschesche H. The metal ion requirement for activation of latent collagenase from human polymorphonuclear leucocytes. Hoppe Seylers Z Physiol Chem. 1981; 362(11):1523–31. https://doi.org/10.1515/bchm2.1981.362.2.1523 PMID: 6273285
6. Hahn PF, Fairman E. The copper content of some human and animal tissues. Journal of Biological Chemistry. 1936; 113(1):161–5.
7. Margalioth EJ, Schenker JG, Chevion M. Copper and zinc levels in normal and malignant tissues. Cancer. 1983; 52(5):868–72. PMID: 6871828
8. Rubino JT, Franz KJ. Coordination chemistry of copper proteins: How nature handles a toxic cargo for essential function. J Inorg Biochem. 2012; 107(1):129–43. https://doi.org/10.1016/j.jinorgbio.2011.11.024 PMID: 22204943
9. Ye S, Wu X, Wei L, Tang DM, Sun P, Bartlam M, et al. An insight into the mechanism of human cysteine dioxygenase—Key roles of the thioether-bonded tyrosine-cysteine cofactor. Journal of Biological Chemistry. 2007; 282(5):3391–402. https://doi.org/10.1074/jbc.M609337200 PMID: 17135237
10. Lentsch AB, Kato A, Saari JT, Schuschke DA. Augmented metalloproteinase activity and acute lung injury in copper-deficient rats. Am J Physiol Lung Cell Mol Physiol. 2001; 281(2):L387–93. https://doi.org/10.1152/ajplung.2001.281.2.L387 PMID: 11435213
11. Parr-Sturgess CA, Tinker CL, Hart CA, Brown MD, Clarke NW, Parkin ET. Copper modulates zinc metalloproteinase-dependent ectodomain shedding of key signaling and adhesion proteins and promotes the invasion of prostate cancer epithelial cells. Mol Cancer Res. 2012; 10(10):1282–93. https://doi.org/10.1158/1541-7786.MCR-12-0312 PMID: 22936788
12. Hwang JJ, Park MH, Koh JY. Copper activates TrkB in cortical neurons in a metalloproteinase-dependent manner. J Neurosci Res. 2007; 85(10):2160–6. PMID: 17520746
13. Heitzer M, Hallmann A. An extracellular matrix-localized metalloproteinase with an exceptional QEXXH metal binding site prefers copper for catalytic activity. J Biol Chem. 2002; 277(31):28280–6. https://doi.org/10.1074/jbc.M203925200 PMID: 12034745
14. McGuffin LJ, Adiyaman R, Maghrabi AHA, Shuid AN, Brackenridge DA, Nealon JO, et al. IntFOLD: an integrated web resource for high performance protein structure and function prediction. Nucleic Acids Res. 2019; 47(W1):W408–W13. https://doi.org/10.1093/nar/gkz322 PMID: 31045208
15. Juurikka K, Butler GS, Salo T, Nyberg P, Astrom P. The Role of MMP8 in Cancer: A Systematic Review. Int J Mol Sci. 2019; 20(18). https://doi.org/10.3390/ijms20184506 PMID: 31514474
16. Coates RJ, Weiss NS, Daling JR, Rettmer RL, Warnick GR. Cancer risk in relation to serum copper levels. Cancer Res. 1989; 49(15):4353–6. PMID: 2743325
17. Denoyer D, Masaldan S, La Fontaine S, Cater MA. Targeting copper in cancer therapy: 'Copper That Cancer'. Metallomics. 2015; 7(11):1459–76. https://doi.org/10.1039/c5mt00149h PMID: 26313539
18. Bode W, Gomis-Ruth FX, Stockler W. Astacins, serralysins, snake venom and matrix metalloproteinases exhibit identical zinc-binding environments (HEXXHXXGXXH and Met-turn) and topologies and should be grouped into a common family, the 'metzincins'. FEBS Lett. 1993; 331(1–2):134–40. PMID: 8405391
19. Tauro M, Laghezza A, Loiodice F, Piemontese L, Caradonna A, Capelli D, et al. Catechol-based matrix metalloproteinase inhibitors with additional antioxidative activity. J Enzyme Inhib Med Chem. 2016; 31(sup4):25–37. https://doi.org/10.1080/14756366.2016.1217853 PMID: 27556138
20. Bertini I, Calderone V, Fragai M, Luchinat C, Maletta M, Yeo KJ. Snapshots of the reaction mechanism of matrix metalloproteinases. Angew Chem Int Ed Engl. 2006; 45(47):7952–5. https://doi.org/10.1002/anie.200603100 PMID: 17096442

21. Pelmenschikov V, Siegbahn PE. Catalytic mechanism of matrix metalloproteinases: two-layered ONIOM study. Inorg Chem. 2002; 41(22):5659–66. https://doi.org/10.1021/ic0255656 PMID: 12401069

22. Lovejoy B, Hassell AM, Luther MA, Weigl D, Jordan SR. Crystal-Structures of Recombinant 19-Kda Human Fibroblast Collagenase Complexed to Itself. Biochemistry-Us. 1994; 33(27):8207–17.

23. Stocker W, Bode W. Structural Features of a Superfamily of Zinc-Endopeptidases—the Metzincins. Curr Opin Struc Biol. 1995; 5(3):383–90. https://doi.org/10.1016/0959-440x(95)80101-4 PMID: 7583637

24. Manka SW, Carafoli F, Visse R, Bihan D, Raynal N, Farndale RW, et al. Structural insights into triple-helical collagen cleavage by matrix metalloproteinase 1. Proc Natl Acad Sci U S A. 2012; 109 (31):12461–6. https://doi.org/10.1073/pnas.1204991109 PMID: 22761315

25. Prior SH, Byrne TS, Tokmina-Roszyk D, Fields GB, Van Doren SR. Path to Collagenolysis: COLLAGEN V TRIPLE-HELIX MODEL BOUND PRODUCTIVELY AND IN ENCOUNTERS BY MATRIX METALLO-PROTEINASE-12. J Biol Chem. 2016; 291(15):7888–901. https://doi.org/10.1074/jbc.M115.703124 PMID: 26887942

26. Koch KA, Pena MM, Thiele DJ. Copper-binding motifs in catalysis, transport, detoxification and signaling. Chem Biol. 1997; 4(8):549–60. https://doi.org/10.1016/s1074-5521(97)90241-6 PMID: 9281528

27. Warren JJ, Lancaster KM, Richards JH, Gray HB. Inner- and outer-sphere metal coordination in blue copper proteins. J Inorg Biochem. 2012; 115:119–26. https://doi.org/10.1016/j.jinorgbio.2012.05.002 PMID: 22658756

28. Nar H, Huber R, Messerschmidt A, Filippou AC, Barth M, Jaquinod M, et al. Characterization and crystal structure of zinc azurin, a by-product of heterologous expression in Escherichia coli of Pseudomonas aeruginosa copper azurin. Eur J Biochem. 1992; 205(3):1123–9. PMID: 1576995

29. Stiebritz MT, Hu Y. Computational Methods for Modeling Metalloproteins. Methods Mol Biol. 2019; 1876:245–66. https://doi.org/10.1007/978-1-4939-8864-8_16 PMID: 30317486

30. Gogoi P, Chandravanshi M, Mandal SK, Srivastava A, Kanaujia SP. Heterogeneous behavior of metalloproteins toward metal ion binding and selectivity: insights from molecular dynamics studies. J Biomol Struct Dyn. 2016; 34(7):1470–85. https://doi.org/10.1080/07391102.2015.1080629 PMID: 26248730

31. Siegbahn PE, Himo F. Recent developments of the quantum chemical cluster approach for modeling enzyme reactions. J Biol Inorg Chem. 2009; 14(5):643–51. https://doi.org/10.1007/s00775-009-0511-y PMID: 19437047

32. Borowski T, Quesne M, Szaleniec M. QM and QM/MM Methods Compared: Case Studies on Reaction Mechanisms of Metalloenzymes. Adv Protein Chem Struct Biol. 2015; 100:187–224. https://doi.org/10.1016/bs.apcsb.2015.06.005 PMID: 26415845

33. Frisch MJ, Trucks GW, Schlegel HB, Scuseria GE, Robb MA, Cheeseman JR, et al. Gaussian, Inc. Wallingford CT2016.

34. Dennington R, Keith T, Millam J. Gauss View. Shawnee Mission: Semichem Inc.; 2009.

35. Boudko SP, Engel J, Okuyama K, Mizuno K, Bachinger HP, Schumacher MA. Crystal structure of human type III collagen Gly991-Gly1032 cystine knot-containing peptide shows both 7/2 and 10/3 triple helical symmetries. J Biol Chem. 2008; 283(47):32580–9. https://doi.org/10.1074/jbc.M805394200 PMID: 18805790

36. Tochowicz A, Maskos K, Huber R, Oltenfreiter R, Dive V, Yiotakis A, et al. Crystal structures of MMP-9 complexes with five inhibitors: contribution of the flexible Arg424 side-chain to selectivity. J Mol Biol. 2007; 371(4):989–1006. https://doi.org/10.1016/j.jmb.2007.05.068 PMID: 17599356

37. Sakharov DV, Lim C. Zn protein simulations including charge transfer and local polarization effects. J Am Chem Soc. 2005; 127(13):4921–9. https://doi.org/10.1021/ja0429115 PMID: 15796557